

Article

# Adsorption Properties of Hydrocarbons (n-Decane, Methyl Cyclohexane and Toluene) on Clay Minerals: An Experimental Study

Jie Zhang <sup>1,2</sup>, Shuangfang Lu <sup>1</sup>, Junqian Li <sup>1,\*</sup> , Pengfei Zhang <sup>1,2</sup>, Haitao Xue <sup>1</sup>, Xu Zhao <sup>3,4</sup> and Liujuan Xie <sup>1,2</sup>

<sup>1</sup> Research Institute of Unconventional Oil & Gas and Renewable Energy, China University of Petroleum (East China), Qingdao 266580, China; zhangjie1994upc@163.com (J.Z.); lushuangfang@upc.edu.cn (S.L.); zhangpengfeiupc@163.com (P.Z.); xueht@upc.edu.cn (H.X.); 1987sarah@163.com (L.X.)

<sup>2</sup> School of Geosciences, China University of Petroleum (East China), Qingdao 266580, China

<sup>3</sup> Exploration & Production Research Institute SINOPEC, Beijing 100083, China; zhaoxu.syky@sinopec.com

<sup>4</sup> Shandong Provincial Key Laboratory of Depositional Mineralization & Sedimentary Mineral, Shandong University of Science and Technology, Qingdao 266590, China

\* Correspondence: lijunqian1987@126.com

Received: 20 September 2017; Accepted: 4 October 2017; Published: 12 October 2017

**Abstract:** Adsorption of hydrocarbons may significantly affect hydrocarbon migration in unconventional reservoirs. Clay minerals form the primary adsorbent surfaces for hydrocarbons adsorbed in mudstone/shale. To study the adsorption properties of hydrocarbons (n-decane (C<sub>10</sub>H<sub>22</sub>), methyl cyclohexane (C<sub>7</sub>H<sub>14</sub>) and toluene (C<sub>7</sub>H<sub>8</sub>)) on clay minerals (i.e., cookeite, ripidolite, kaolinite, illite, illite/smectite mixed-layer, Na-montmorillonite and Ca-montmorillonite), hydrocarbon vapor adsorption (HVA) tests were conducted at 298.15 K. The results showed that (i) the adsorption amounts of C<sub>10</sub>H<sub>22</sub>, C<sub>7</sub>H<sub>14</sub> and C<sub>7</sub>H<sub>8</sub> ranged from 0.45–1.03 mg/m<sup>2</sup>, 0.28–0.90 mg/m<sup>2</sup> and 0.16–0.53 mg/m<sup>2</sup>, respectively; (ii) for cookeite, ripidolite and kaolinite, the adsorption capacity of C<sub>10</sub>H<sub>22</sub> was less than C<sub>7</sub>H<sub>14</sub>, which was less than C<sub>7</sub>H<sub>8</sub>; (iii) for illite, Na-montmorillonite and Ca-montmorillonite, the adsorption capacity of C<sub>10</sub>H<sub>22</sub> was greater than that of C<sub>7</sub>H<sub>8</sub>, and the adsorption capacity of C<sub>7</sub>H<sub>14</sub> was the lowest; (iv) for an illite/smectite mixed-layer, C<sub>7</sub>H<sub>14</sub> had the highest adsorption capacity, followed by C<sub>10</sub>H<sub>22</sub>, and C<sub>7</sub>H<sub>8</sub> had the lowest capacity. Adsorption properties were correlated with the microscopic parameters of pores in clay minerals and with experimental pressure. Finally, the weighted average method was applied to evaluate the adsorption properties of C<sub>10</sub>H<sub>22</sub>, C<sub>7</sub>H<sub>14</sub> and C<sub>7</sub>H<sub>8</sub> on clay minerals in oil-bearing shale from the Shahejie Formation of Dongying Sag in the Bohai Bay Basin, China. For these samples, the adsorbed amounts of C<sub>7</sub>H<sub>14</sub> ranged from 18.03–28.02 mg/g (mean 23.33 mg/g), which is larger than that of C<sub>10</sub>H<sub>22</sub>, which ranges from 15.40–21.72 mg/g (mean 18.82 mg/g). The adsorption capacity of C<sub>7</sub>H<sub>8</sub> was slightly low, ranging from 10.51–14.60 mg/g (mean 12.78 mg/g).

**Keywords:** hydrocarbon vapor adsorption (HVA); adsorption property; n-decane; methyl cyclohexane; toluene; clay minerals

## 1. Introduction

The adsorption of hydrocarbons may affect hydrocarbon migration in the subsurface [1], which significantly impacts the recovery from unconventional reservoirs [2–6]. Clay minerals form the primary adsorbent surface for adsorbed hydrocarbons in mudstone/shale [7–10]. In recent decades, the adsorption behavior of CH<sub>4</sub> on clay minerals has been studied extensively in a large number of laboratory experiments [11–14]. In addition to CH<sub>4</sub>, a few studies were conducted

using  $C_2H_2$  [11,12], and a gas mixture of  $C_1$ – $C_6$  alkanes [15]. It is generally considered that  $CH_4$  adsorption capacity of clay minerals is determined by its pore volume and specific surface area [16,17]. However, due to the dramatic differences in physicochemical properties between liquid and gas, previously proposed techniques [14,18–25] and models (including Freundlich [26,27], Langmuir [28], and Dubinin-Astakhov [29–31]) for gas adsorption are not appropriate to evaluate hydrocarbon in a liquid state.

Usually, hydrocarbon-solution adsorption tests were used to determine adsorption capacity of liquid hydrocarbon on porous media [32–45]. First, mixed hydrocarbons (e.g., crude oil, asphaltene, maltene and resin) are diluted using an organic solvent (e.g., toluene and n-heptane) to a certain concentration. Then, experiments are carried out to determine the adsorption capacity of minerals (e.g., clay minerals, quartz, feldspar, calcite and dolomite) as a function of equilibrium time or hydrocarbon concentration under a certain temperature. Previous studies showed the following: (1) for shale-oil, clay minerals had the highest adsorption capacity (18.0 mg/g), quartz had an intermediate value (3.0 mg/g), and carbonates had the lowest adsorption capacity (1.8 mg/g) [39]; (2) for quartz, the adsorbed amount (2 mg/g) of asphaltene [36], which was diluted with a solution of n-heptane and toluene, is apparently lower than that of asphaltene diluted with toluene (4.5 mg/g) [45] and 6.4 mg/g [44]; (3) feldspar has a greater adsorption capacity than quartz [45]; (4) for calcite, the maximum adsorbed amount of polar compounds (resin and asphaltene) is 2.1–3.6 mg/g [42]; and (5) when compared to limestone, dolomite has a smaller adsorption capacity and a smaller adsorbed amount of asphaltene diluted in toluene [46].

Examination of the adsorption behavior of a hydrocarbon solution should consider the interactions of the adsorbent, solute (i.e., adsorbate) and solvent. Usually, greater interaction between the adsorbent and solute results in a larger adsorption capacity. Nevertheless, interaction between the solute and solvent can prevent the adsorbent adsorbing the solute from the solvent, negatively affecting the adsorption process. These complexities require a new method to study adsorption properties of liquid hydrocarbons on clay minerals.

In order to account for the complex constituent clay minerals in oil-bearing mudstone/shale, we use hydrocarbon vapor adsorption (HVA) tests to evaluate the adsorption properties of hydrocarbons (n-decane ( $C_{10}H_{22}$ ), methyl cyclohexane ( $C_7H_{14}$ ) and toluene ( $C_7H_8$ )) on different clay minerals (i.e., cookeite, ripidolite, kaolinite, illite, illite/smectite mixed-layer, Na-montmorillonite and Ca-montmorillonite) by obtaining adsorption isotherms with increasing relative pressure at 298.15 K [47,48]. Furthermore, we investigate the impact of microscopic parameters (specific surface area, pore size distribution, pore volume, etc.) related to pores in clay minerals and pressure on the adsorption properties of  $C_{10}H_{22}$ ,  $C_7H_{14}$  and  $C_7H_8$  on clay minerals. Finally, we evaluate the adsorption properties of  $C_{10}H_{22}$ ,  $C_7H_{14}$  and  $C_7H_8$  on clay minerals in oil-bearing shale from the Shahejie Formation of the Dongying Sag in the Bohai Bay Basin, northern China.

## 2. Materials and Methods

### 2.1. Materials

The pure clay minerals of cookeite (CAr-1), ripidolite (CCa-2), kaolinite (KGA-1b), illite (IMt-2), illite/smectite mixed-layer (ISCz-1), Na-montmorillonite (SWy-2) and Ca-montmorillonite (STx-1b) were obtained from the Clay Minerals Society. Baseline Studies (e.g., composition, geologic origin, infrared (IR) analysis, thermal analysis, chemical analysis and cation exchange capacity) of clay minerals from the Clay Minerals Society are available [49–58].

Oil-bearing shale samples (B172, F169, F41, H172, H88, L76, LX884 and Y556) were obtained from the primary shale formations of different petroleum well boreholes in the Dongying sag of the Bohai Bay basin, China. In the sag, the development of lacustrine mudstone/shale formations was widespread in the Eocene Shahejie Formation, mainly including the Middle and Lower-third Member ( $Es_3^z$  and  $Es_3^x$ ) and the Upper-fourth Member ( $Es_4^s$ ). As one of the prospective districts in China

for shale oil development, abundant oil-gas resources have been discovered recently in the shale formations from the  $Es_3^x$  and  $Es_4^s$  sub-members of the sag [48].

All clay samples were milled into powder particles at 40–60 mesh (250–425  $\mu\text{m}$ ) by an agate mortar. Then, each sample was subdivided into three parts, which were tested for HVA, low-temperature nitrogen adsorption/desorption (LT- $\text{N}_2\text{A/D}$ ) and low-pressure carbon dioxide adsorption (LP- $\text{CO}_2\text{A}$ ). The objective of these tests was to obtain the adsorption isotherms of hydrocarbons and the microscopic parameters of pores in clay minerals.

## 2.2. HVA Test

HVA tests were conducted for the n-decane ( $\text{C}_{10}\text{H}_{22}$ ), methyl cyclohexane ( $\text{C}_7\text{H}_{14}$ ) and toluene ( $\text{C}_7\text{H}_8$ ) adsorption on clay minerals using a 3H-2000PW Gravimetry Vapor Sorption Analyzer [48]. Prior to the test, the samples were heated at 383.15 K to remove residual gas and water in the sample [59–61]. The equipment and procedure used here is the same as that used in HVA tests of  $\text{C}_{10}\text{H}_{22}$  at a certain relative pressure that are detailed in a previous study by Li et al. [48]. In this study, the experimental temperature is held constant at 298.15 K. Because it is difficult to precisely control the experimental pressure due to the large carbon numbers of the hydrocarbons, adsorption isotherms for  $\text{C}_{10}\text{H}_{22}$ ,  $\text{C}_7\text{H}_{14}$  and  $\text{C}_7\text{H}_8$  were only measured at several non-uniform relative pressure points. The highest relative pressures ( $P/P_0$ ) measured were 0.8  $P/P_0$  for  $\text{C}_{10}\text{H}_{22}$  and 0.9  $P/P_0$  for  $\text{C}_7\text{H}_{14}$  and  $\text{C}_7\text{H}_8$ . Under 0.8  $P/P_0$  and 298.15 K conditions, the total amount ( $Q_t$ ) of  $\text{C}_{10}\text{H}_{22}$  accumulating on clay minerals was measured. Under 0.9  $P/P_0$  and 298.15 K conditions, the total amounts ( $Q_t$ ) of  $\text{C}_7\text{H}_{14}$  and  $\text{C}_7\text{H}_8$  were obtained.

## 2.3. LT- $\text{N}_2\text{A/D}$ and LP- $\text{CO}_2\text{A}$ Tests

LT- $\text{N}_2\text{A/D}$  isotherms were measured over relative pressures ranging from approximately  $10^{-5}$  to 0.995 using an Autosorb-iQ-Station-1 instrument at 77 K [48] to obtain the pore size distributions (PSD), pore volumes and specific surface areas of the clay minerals. The maximum pore diameter ( $d_{\text{max}}$ ) (306.42–385.55 nm) was directly determined by Barrett-Joyner-Halenda (BJH) method [62]. The minimum pore diameter ( $d_{\text{min}}$ ) (1.17–1.22 nm) was obtained by density functional theory (DFT) [63]. In addition, LP- $\text{CO}_2\text{A}$  tests were carried out on an Autosorb-iQ-MP instrument at 273.15 K to obtain the pore size distribution of pores with the size of 0.305–1.475 nm. According to the classification of the International Union of Pure and Applied Chemistry (IUPAC), pores were subdivided into micropores (<2 nm in diameter), mesopores (2–50 nm in diameter) and macropores (>50 nm in diameter) [64]. LT- $\text{N}_2\text{A/D}$  and LP- $\text{CO}_2\text{A}$  tests referred to the People's Republic of China petroleum natural gas profession standard (SY/T 6154-1995) and National Standards of the People's Republic of China (GBT 21650.3-2011), respectively.

## 2.4. XRD

The constituent clay minerals of the oil-bearing shale samples (B172, F169, F41, H172, H88, L76, LX884 and Y556) were analyzed using a Bruker D8 DISCOVER X-ray diffraction at 295.15 K temperature and 35% humidity. The radiation source was Cu.

# 3. Results and Discussion

## 3.1. Adsorption Properties of $\text{C}_{10}\text{H}_{22}$ , $\text{C}_7\text{H}_{14}$ and $\text{C}_7\text{H}_8$ on Clay Minerals

The amount of hydrocarbon measured during the tests contains two parts: adsorption and capillary condensation. As shown in Figure 1, from the  $P/P_0 \approx 0$ , the amount of hydrocarbons adsorbed by clay minerals made up most of the total amount of hydrocarbon measured during the tests and is closely related to the specific surface area of clay minerals. With increasing relative pressure ( $0 < P/P_0 < 1$ ), capillary condensation begins to appear on the interspace of pores. At relatively high pressures, condensed rather than adsorbed hydrocarbon became the larger contributor to the

total amount of hydrocarbon measured during the tests. Accordingly, at certain relative pressures (i.e., inflection points), the amount of hydrocarbon measured per unit surface area ( $n_{BET}$ ) accurately reflects the adsorption of hydrocarbons on clay minerals, and the values of  $n_{BET}$  are assumed to be the adsorbed amount per unit surface area.

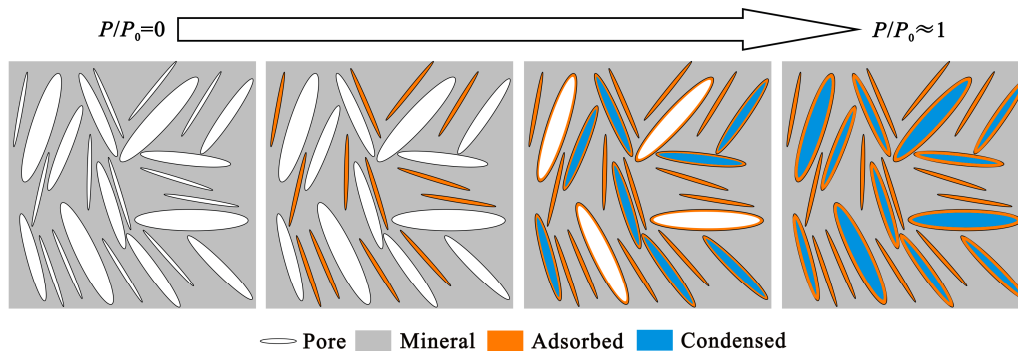


**Figure 1.** Schematic of the adsorption and condensation of hydrocarbon with increasing relative pressure.

As shown in Figure 2, correlation coefficients ( $R^2$ ) between BET surface areas ( $A_{BET}$ ) and tested amounts of hydrocarbon ( $Q$ ) for  $C_{10}H_{22}$ ,  $C_7H_{14}$  and  $C_7H_8$  increase linearly at the early stages of pressure increase, but then deviate from the straight lines (even decreasing for  $C_{10}H_{22}$  and  $C_7H_8$ ). These inflection points occur at approximately  $0.65 P/P_0$  ( $C_{10}H_{22}$ ),  $0.4 P/P_0$  ( $C_7H_{14}$ ) and  $0.3 P/P_0$  ( $C_7H_8$ ). Theoretically, high  $R^2$  values reflect the dominance of the adsorption process of hydrocarbons on pore surfaces, and low  $R^2$  values are mainly attributed to the apparent dominance of capillary condensation. As shown in Figure 2a–c, the correlation coefficient ( $R^2$ ) for total pore volume ( $V_t$ ) and tested amount of hydrocarbon ( $Q$ ) continues to increase when  $P/P_0$  is larger than the inflection point. If capillary condensation had no effect, then the  $R^2$  values for  $V_t$  and  $Q$  would decrease with decreasing  $R^2$  values for  $A_{BET}$  and  $Q$  because total pore volume is proportional to BET surface area (Figure 3a). In Figure 2b, as  $P/P_0$  becomes larger than the  $P/P_0$  at the inflection point, the value of the correlation coefficient ( $R^2$ ) of  $A_{BET}$  and  $Q$  does not decrease but deviates from the straight line. For  $C_7H_{14}$ , the capillary condensation may not be strong enough to cause the decrease in  $R^2$  value, since when compared with  $C_{10}H_{22}$  and  $C_7H_8$ ,  $C_7H_{14}$  has the smallest radius of capillary condensation according to the classical Kelvin equation [65]. Therefore, at the inflection points, the amount of hydrocarbon per unit surface area measured during the test (i.e.,  $n_{BET}$ ) (Table 1) can be used to evaluate the adsorption properties of hydrocarbons on clay minerals.

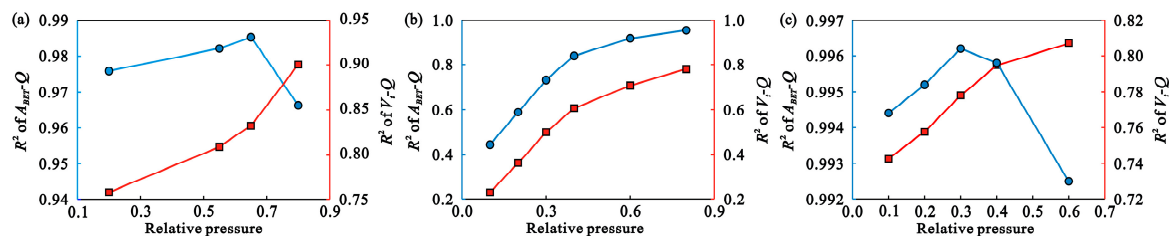


**Figure 2.** Correlation coefficients for BET surface area and tested hydrocarbon amount ( $R^2$  of  $A_{BET}-Q$ ) shown with blue line and Y-axis, and correlation coefficients for total pore volume and tested hydrocarbon amount ( $R^2$  of  $V_t-Q$ ) shown with red line and Y-axis for  $C_{10}H_{22}$  (a),  $C_7H_{14}$  (b) and  $C_7H_8$  (c) with increasing relative pressure.

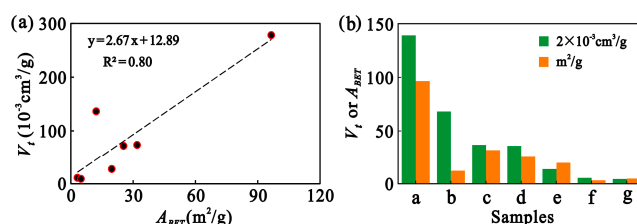


**Figure 3.** (a) Relationship between BET surface areas ( $A_{BET}$ ) and total pore volumes ( $V_t$ ) of clay minerals; (b) total pore volumes ( $V_t$ ) and BET surface areas ( $A_{BET}$ ) of clay minerals from LT-N<sub>2</sub>A/D tests (a–g: Ca-montmorillonite, kaolinite, illite/smectite mixed-layer, Na-montmorillonite, illite, cookeite and ripidolite).

**Table 1.** Tested amounts ( $q_a$ ) of C<sub>10</sub>H<sub>22</sub>, C<sub>7</sub>H<sub>14</sub> and C<sub>7</sub>H<sub>8</sub> measured at inflection points and the  $q_a$  per unit of surface area ( $n_{BET}$ ) for clay minerals.

Clay Minerals	Codes	$n_{BET}$ (mg/m <sup>2</sup> )			$q_a$ (mg/g)		
		C <sub>10</sub> H <sub>22</sub>	C <sub>7</sub> H <sub>14</sub>	C <sub>7</sub> H <sub>8</sub>	C <sub>10</sub> H <sub>22</sub>	C <sub>7</sub> H <sub>14</sub>	C <sub>7</sub> H <sub>8</sub>
cookeite	CAr-1	1.02	0.28	0.16	3.32 ± 0.05	0.91 ± 0.01	0.53 ± 0.02
ripidolite	CCa-2	0.45	0.36	0.31	2.24 ± 0.01	1.81 ± 0.01	1.52 ± 0.02
kaolinite	KGa-1b	0.73	0.34	0.23	8.90 ± 0.23	4.21 ± 0.02	2.85 ± 0.13
illite	IMt-2	0.46	0.36	0.40	9.03 ± 0.03	7.03 ± 0.01	7.92 ± 0.04
illite/smectite mixed-layer	ISCz-1	0.69	0.90	0.46	22.11 ± 0.08	28.67 ± 0.02	14.81 ± 0.03
Na-montmorillonite	SWy-2	0.53	0.29	0.41	13.58 ± 0.06	7.45 ± 0.01	10.43 ± 0.04
Ca-montmorillonite	STx-1b	0.83	0.42	0.53	80.24 ± 0.19	40.82 ± 0.04	51.47 ± 0.19

For C<sub>10</sub>H<sub>22</sub>, the values of  $n_{BET}$  range from 0.45–1.03 mg/m<sup>2</sup> (mean 0.67 mg/m<sup>2</sup>). Cookeite has the greatest adsorption of C<sub>10</sub>H<sub>22</sub>, followed by Ca-montmorillonite. For C<sub>7</sub>H<sub>14</sub>, the values of  $n_{BET}$  range from 0.28–0.90 mg/m<sup>2</sup>, with an average of 0.42 mg/m<sup>2</sup>. The interaction between C<sub>7</sub>H<sub>14</sub> and the illite/smectite mixed-layer is the most prominent among all the clay minerals. When compared with C<sub>10</sub>H<sub>22</sub> and C<sub>7</sub>H<sub>14</sub>, the adsorption of C<sub>7</sub>H<sub>8</sub> on clay minerals is relatively weak, with a range of 0.16–0.53 mg/m<sup>2</sup> (mean 0.35 mg/m<sup>2</sup>). For C<sub>7</sub>H<sub>8</sub>, Ca-montmorillonite has the largest  $n_{BET}$  (0.53 mg/m<sup>2</sup>), illite/smectite mixed-layer has the second largest value (0.46 mg/m<sup>2</sup>), and cookeite has the lowest adsorption value (0.16 mg/m<sup>2</sup>). The hydrocarbon amounts ( $q_a$ ) tested at inflection points are shown in Table 1. Apparently, the adsorption capacities of C<sub>10</sub>H<sub>22</sub>, C<sub>7</sub>H<sub>14</sub> and C<sub>7</sub>H<sub>8</sub> on clay minerals are diverse: (a) for cookeite, ripidolite and kaolinite, the adsorption capacities for C<sub>10</sub>H<sub>22</sub>, C<sub>7</sub>H<sub>14</sub> and C<sub>7</sub>H<sub>8</sub> progressively decrease for all the clay minerals; (b) for illite, Na-montmorillonite and Ca-montmorillonite, the adsorption capacity of C<sub>10</sub>H<sub>22</sub> is greater than that of C<sub>7</sub>H<sub>8</sub>, which is greater than C<sub>7</sub>H<sub>14</sub>; (c) for the illite/smectite mixed-layer, C<sub>7</sub>H<sub>14</sub> has the highest adsorption capacity, followed by C<sub>10</sub>H<sub>22</sub>, and the C<sub>7</sub>H<sub>8</sub> has the lowest capacity.

When the phenomenon of capillary condensation is considered [66], the amount of hydrocarbon measured at a certain  $P/P_0$  includes both the adsorbed and condensed (i.e., free-phase-like liquid) hydrocarbon. Thus, the hydrocarbons measured at each experimental point represent the accumulated amount in clay minerals, which includes adsorbed and free hydrocarbons. As  $P/P_0$  becomes extremely high, up to ~1, pore spaces will become completely filled with hydrocarbon in adsorbed and condensed states [48]. In this paper, the tested amounts ( $Q$ ) of C<sub>10</sub>H<sub>22</sub>, C<sub>7</sub>H<sub>14</sub> and C<sub>7</sub>H<sub>8</sub> with increasing  $P/P_0$  are expressed in Figure 4; the accumulated amount of hydrocarbons in clay minerals increases with increasing  $P/P_0$ . The accumulated amounts of C<sub>10</sub>H<sub>22</sub> in clay minerals are presented in Figure 4a. At  $P/P_0 = 0.8$ , (a) the accumulated amount of hydrocarbon in Ca-montmorillonite is the largest, over 100 mg/g; (b) the accumulated amounts in Na-montmorillonite, the illite/smectite mixed-layer and kaolinite progressively decrease, ranging from 33.89–25.46 mg/g; (c) illite has a relatively low accumulated amount (14.09 mg/g); (d) the accumulated amount for cookeite is slightly higher than that of ripidolite, but both are extremely low with an average value of 4.31 mg/g. In Figure 4b–c,

the amounts of  $C_7H_{14}$  and  $C_7H_8$  accumulated in clay minerals are presented. At  $P/P_0 = 0.9$ , the accumulated amount of  $C_7H_{14}$  and  $C_7H_8$  in Ca-montmorillonite is more than 100 mg/g, much higher than the accumulation amounts in the other clay minerals. For  $C_7H_8$ , Na-montmorillonite has a greater storage capacity than the illite/smectite mixed-layer, whereas for  $C_7H_{14}$ , the result is the opposite. The mean accumulated amount of  $C_7H_{14}$  and  $C_7H_8$  in kaolin is 21.05 mg/g, which is larger than the value (15.87 mg/g) for illite. Ripidolite has an extremely weak storage capacity of  $C_7H_{14}$  and  $C_7H_8$ , with an average of 3.69 mg/g, which is slightly greater than that of cookeite (2.98 mg/g).

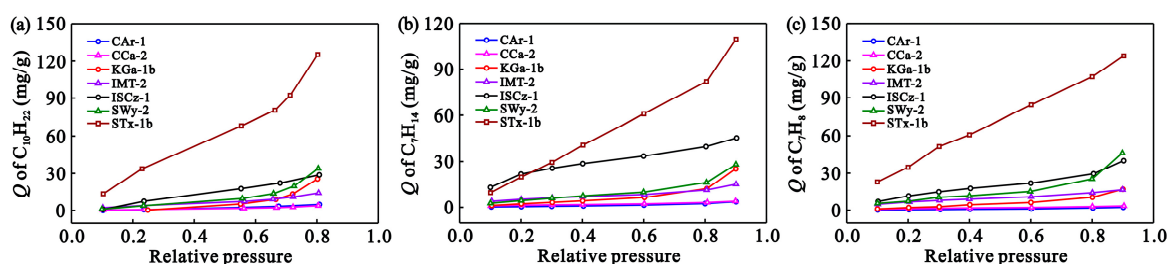


**Figure 4.** Tested amounts ( $Q$ ) of  $C_{10}H_{22}$  (a),  $C_7H_{14}$  (b) and  $C_7H_8$  (c) with increasing  $P/P_0$  for clay minerals (CAr-1: cookeite; CCa-2: ripidolite; KGa-1b: kaolinite; IMT-2: illite; ISCz-1: illite/smectite mixed-layer; SWy-2: Na-montmorillonite; STx-1b: Ca-montmorillonite).

Therefore, in terms of relative amounts of accumulated hydrocarbons for  $C_{10}H_{22}$ ,  $C_7H_{14}$  and  $C_7H_8$ : Ca-montmorillonite  $\gg$  illite/smectite mixed-layer and Na-montmorillonite > kaolinite > illite > cookeite and ripidolite, which is different from the  $CH_4$  adsorption capacity: montmorillonite  $\gg$  illite/smectite mixed-layer > kaolinite > chlorite > illite, as reported by Ji et al. [13].

### 3.2. Factors Influencing Hydrocarbon Adsorption on Clay Minerals

Microscopically, adsorption/desorption of hydrocarbon molecules on the surface of clay minerals is influenced by the intermolecular force. In addition, if the clay minerals adsorb hydrocarbon molecules, adsorption sites on the surface must be present. Therefore, the adsorption properties of  $C_{10}H_{22}$ ,  $C_7H_{14}$  and  $C_7H_8$  are associated with the microscopic parameters (specific surface area, pore size distribution, pore volume, etc.) of pores in clay minerals, as well as the experimental conditions (temperature and pressure, etc.).

#### 3.2.1. Microscopic Parameters of Pores in Clay Minerals

The adsorption properties of  $C_{10}H_{22}$ ,  $C_7H_{14}$  and  $C_7H_8$  are associated with the microscopic parameters (specific surface area, pore size distribution, pore volume, etc.) of pores in clay minerals. In this study, the total pore volumes were measured by LT- $N_2$ A/D tests. The specific surface area was calculated from the adsorption branch of the  $N_2$  isotherm by the standard Brunauer-Emmett-Teller (BET) equation with relative pressure ranging from 0.05 to 0.3 [67]. Because of an extraneous peak located at  $\sim 3.8$  nm in the PSD curves obtained using the BJH method [68], the PSDs ( $>1.475$  nm in diameter) were determined by combining the DFT with BJH method using LT- $N_2$ A/D tests, and other PSDs ( $<1.475$  nm in diameter) were obtained by LP- $CO_2$ A tests.

As shown in Figure 3b and Table 2, the BET surface areas ( $A_{BET}$ ) range from 3.242–96.563  $m^2/g$  (mean 27.731  $m^2/g$ ). Ca-montmorillonite has the largest specific surface area followed by the illite/smectite mixed-layer (31.959  $m^2/g$ ) and Na-montmorillonite (25.421  $m^2/g$ ). The BET surface areas for Ca- and Na- montmorillonite measured in this study are credible based on comparison with the BET surface areas (24.7–97  $m^2/g$ ) of montmorillonite previously measured [11,69–73]. For illite and kaolinite, the BET surface areas (19.738  $m^2/g$  and 12.271  $m^2/g$ , respectively) decrease progressively but are larger than that of illite (17.5  $m^2/g$ ) [74] and kaolinite (13.0  $m^2/g$ ) [44]. Ripidolite (4.922  $m^2/g$ ) has a slightly higher specific surface area than cookeite (3.242  $m^2/g$ ) and

is similar to chlorite with an  $A_{BET}$  of  $4.8 \text{ m}^2/\text{g}$  as measured by Ross and Bustin [72]. Meanwhile, total pore volumes range from  $8.9 \times 10^{-3}$ – $278.2 \times 10^{-3} \text{ cm}^3/\text{g}$  (mean  $86.8 \times 10^{-3} \text{ cm}^3/\text{g}$ ). Ca-montmorillonite has the largest pore volume followed by kaolinite ( $136.38 \times 10^{-3} \text{ cm}^3/\text{g}$ ). The total pore volume ( $73.75 \times 10^{-3} \text{ cm}^3/\text{g}$ ) of the illite/smectite mixed-layer is approximately the same as that of Na-montmorillonite ( $71.96 \times 10^{-3} \text{ cm}^3/\text{g}$ ) and is significantly larger than that of illite ( $27.53 \times 10^{-3} \text{ cm}^3/\text{g}$ ). Cookeite and ripidolite both have the lowest  $V_t$  ( $11.08 \times 10^{-3}$  and  $8.95 \times 10^{-3} \text{ cm}^3/\text{g}$ , respectively). Thus, in the terms of relative specific surface areas and total pore volumes for clay minerals: Ca-montmorillonite > illite/smectite mixed-layer > Na-montmorillonite > illite > cookeite and ripidolite.

**Table 2.** BET surface areas ( $A_{BET}$ ), total pore volumes ( $V_t$ ) and the percentages of pore volumes from micropore, mesopore and macropore.

Clay Minerals	Codes	$A_{BET}$ ( $\text{m}^2/\text{g}$ )	$V_t$ ( $10^{-3} \text{ cm}^3/\text{g}$ )	Percentages of Pore Volumes (%)		
				Micropore	Mesopore	Macropore
cookeite	CAR-1	3.24	11.08	8.99	65.41	25.61
ripidolite	CCa-2	4.92	8.95	23.29	39.14	37.58
kaolinite	KGa-1b	12.27	136.38	2.68	23.46	73.86
illite	IMt-2	19.74	27.53	24.85	54.86	20.29
illite/smectite mixed-layer	ISCz-1	31.96	73.75	8.03	66.16	25.81
Na-montmorillonite	SWy-2	25.42	71.96	11.90	52.36	35.75
Ca-montmorillonite	STX-1b	96.56	278.17	7.82	55.92	36.26

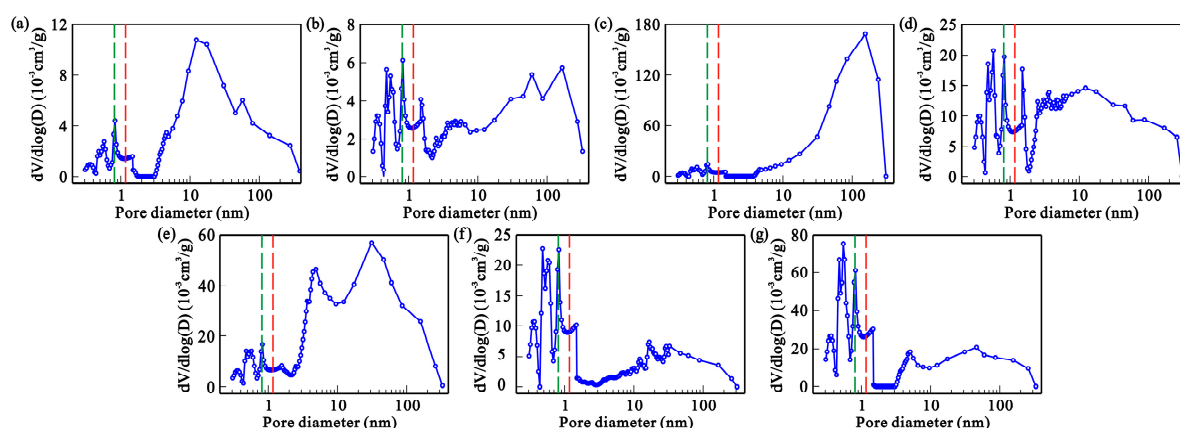


**Figure 5.** Pore size distribution for clay minerals from LT-N<sub>2</sub>A/D and LP-CO<sub>2</sub>A tests (a–g: cookeite, ripidolite, kaolinite, illite, illite/smectite mixed-layer, Na-montmorillonite and Ca-montmorillonite; green short dash line: Pore diameter = 0.82 nm; red short dash line: Pore diameter = 1.17 nm).

There is a part of pore volume ( $V_0$ ) that is inactive and scarcely contributes to hydrocarbon adsorption because the pore diameters are less than the size of hydrocarbon molecules ( $d_0$ ). When considering the complete entrance of molecule into the pore,  $d_0$  should be determined by the maximal length of  $n$ -alkane molecule rather than the cross-sectional diameter. The maximal length of  $n$ -butane ( $\text{C}_4\text{H}_{10}$ ) molecule is 0.8 nm and that of  $n$ -hexane ( $\text{C}_6\text{H}_{14}$ ) is 1.1 nm [75]. The three-dimensional size of a toluene ( $\text{C}_7\text{H}_8$ ) molecule is  $0.380 \times 0.666 \times 0.818 \text{ nm}$  in its minimum energy configuration determined using Material Studio from Accelrys Inc., San Diego, CA, USA. Methyl cyclohexane ( $\text{C}_7\text{H}_{14}$ ) and toluene ( $\text{C}_7\text{H}_8$ ) are both composed of a six-membered carbocyclic ring (cyclohexane or benzene) and a methyl group ( $-\text{CH}_3$ ). The cross-sectional area of cyclohexane is similar to that of benzene [76], thus the maximal length of  $\text{C}_7\text{H}_{14}$  is approximately equal to that of  $\text{C}_7\text{H}_8$ . Consequently, the molecule sizes of  $\text{C}_{10}\text{H}_{22}$ ,  $\text{C}_7\text{H}_{14}$  and  $\text{C}_7\text{H}_8$  are larger than 1.1 nm, 0.818 nm and 0.818 nm, respectively. The volume of micropores (0.82–1.17 nm in diameter) (Figure 5) for clay minerals determined by the LP-CO<sub>2</sub>A test only accounts for an average of 3.16% of the total pore volume

measured using LT-N<sub>2</sub>A/D tests. For the reasons given above, the pore volume of micropores can be simply measured by LT-N<sub>2</sub>A/D tests. Deviations due to the exclusion of pores with sizes between  $d_0$  and  $d_{\min}$  are insignificant and are considered negligible in this paper.

As mentioned previously, the adsorption capacities of C<sub>10</sub>H<sub>22</sub>, C<sub>7</sub>H<sub>14</sub> and C<sub>7</sub>H<sub>8</sub> are closely associated with the specific surface areas of the clay minerals, with correlation coefficients ( $R^2$ ) of 0.985, 0.840 and 0.996, respectively (Figure 2). The relationship between the adsorbed amounts ( $q_a$ ) of C<sub>10</sub>H<sub>22</sub>, C<sub>7</sub>H<sub>14</sub> and C<sub>7</sub>H<sub>8</sub> and the pore volume for micropores, mesopores and macropores measured using LT-N<sub>2</sub>A/D tests are shown in Figure 6. The adsorbed amounts ( $q_a$ ) are proportional to the pore volumes of mesopores rather than that of micropores or macropores. The percentages of active micropores in clay minerals are too small, considering the diameter of *n*-decane, methyl cyclohexane and toluene molecules; in macropores, hydrocarbons are main capillary condensed rather than adsorbed; most clay minerals are dominated by mesopores, thus the adsorbed hydrocarbons mainly exist in mesopores.

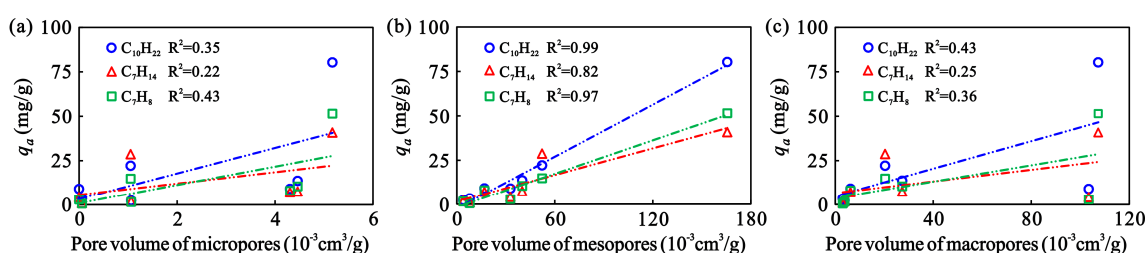


**Figure 6.** Relationships between the adsorbed amounts ( $q_a$ ) and the pore volume of micropores (a), mesopores (b) and macropores (c).

### 3.2.2. Pressure

The adsorption properties of C<sub>10</sub>H<sub>22</sub>, C<sub>7</sub>H<sub>14</sub> and C<sub>7</sub>H<sub>8</sub> on clay minerals are closely associated with the experimental conditions (temperature and pressure, etc.) during HVA tests. In this study, the experimental temperature was held constant at 298.15 K, and the relative pressure ( $P/P_0$ ) varied between 0 and 1. As shown in Figure 7, for one clay mineral sample (i.e., same microscopic parameters of pores), the features of three curves of C<sub>10</sub>H<sub>22</sub>, C<sub>7</sub>H<sub>14</sub> and C<sub>7</sub>H<sub>8</sub> are different. When considering series of samples with the same radius of capillary condensation (i.e., synchronous processes of capillary condensation), the differences and relative changes in the amount of hydrocarbon tested are mainly controlled by the change of adsorption properties with increasing relative pressures.

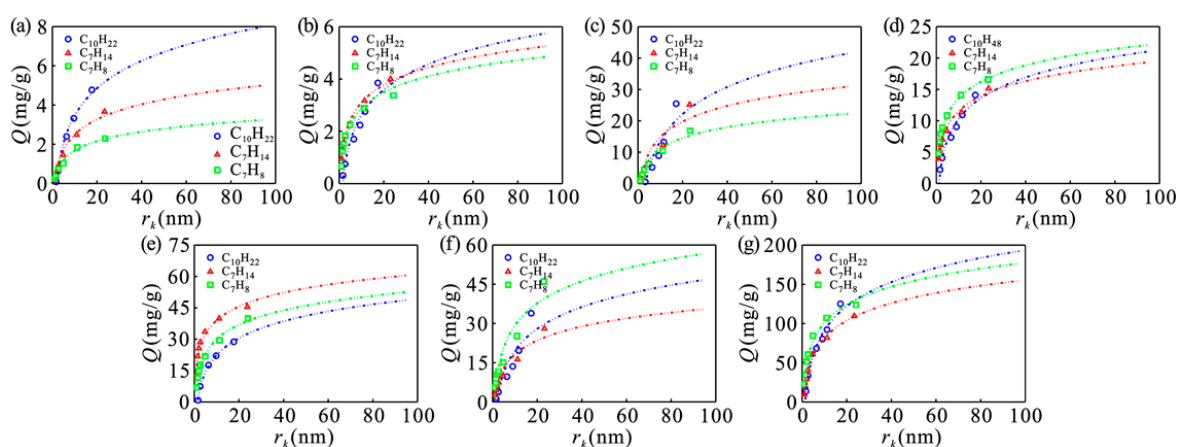


**Figure 7.** Relationship between radius of capillary condensation ( $r_k$ ) and the tested amounts ( $Q$ ) of C<sub>10</sub>H<sub>22</sub>, C<sub>7</sub>H<sub>14</sub> and C<sub>7</sub>H<sub>8</sub> (a–g: cookeite, ripidolite, kaolinite, illite, illite/smectite mixed-layer, Na-montmorillonite and Ca-montmorillonite).

The radius of capillary condensation ( $r_k$ ) as a function of relative pressure ( $P/P_0$ ) was obtained from the classical Kelvin equation [65]:

$$\ln P/P_0 = -\frac{2\sigma V_L}{r_k RT} \cos \theta \quad (1)$$

where  $\sigma$  and  $V_L$  are the surface tension and molar volume of the liquid, measured in dyne/cm and  $\text{m}^3/\text{mol}$ , respectively;  $R$  is the gas constant,  $8.314 \text{ m}^3 \cdot \text{Pa}/(\text{K} \cdot \text{mol})$ ;  $T$  is the absolute temperature, K; and  $\theta$  is the contact angle, which is commonly taken to be zero since the liquid hydrocarbon is assumed to completely wet the adsorbed film. As shown in Figure 7, the tested amounts of  $\text{C}_{10}\text{H}_{22}$ ,  $\text{C}_7\text{H}_{14}$  and  $\text{C}_7\text{H}_8$  on clay minerals are considered as a function of Kelvin radius, which was fitted to Equation (2) using a least square method in IBM SPSS Statistics software

$$Q = a \ln(r_k) + b \quad (2)$$

where  $Q$  is the tested amount of hydrocarbon at the Kelvin radius  $r_k$ . A series of fitting parameters ( $a$ ,  $b$ ) for  $\text{C}_{10}\text{H}_{22}$ ,  $\text{C}_7\text{H}_{14}$  and  $\text{C}_7\text{H}_8$  are shown in Table 3. The parameter  $a$  can effectively represent the differences and relative changes of adsorption properties with increasing  $r_k$  (or  $P/P_0$ ). Comparing the value of  $a$ , clay minerals can be subdivided into Groups A, B and C. Cookeite, ripidolite and kaolinite are in Group A where the parameter  $a$  varies as follows:  $\text{C}_{10}\text{H}_{22} > \text{C}_7\text{H}_{14} > \text{C}_7\text{H}_8$ . Illite, the illite/smectite mixed-layer and Ca-montmorillonite are in Group B where the parameter  $a$  is  $\text{C}_{10}\text{H}_{22} > \text{C}_7\text{H}_8 > \text{C}_7\text{H}_{14}$ . Na-montmorillonite is in Group C where the parameter  $a$  is  $\text{C}_7\text{H}_8 > \text{C}_{10}\text{H}_{22} > \text{C}_7\text{H}_{14}$ .

**Table 3.** Fitting parameters  $a$  and  $b$  for  $\text{C}_{10}\text{H}_{22}$ ,  $\text{C}_7\text{H}_{14}$  and  $\text{C}_7\text{H}_8$ .

Clay Minerals	Codes	$\text{C}_{10}\text{H}_{22}$		$\text{C}_7\text{H}_{14}$		$\text{C}_7\text{H}_8$	
		$a$	$b$	$a$	$b$	$a$	$b$
cookeite	CAR-1	2.013	-1.172	1.113	-0.068	0.695	0.074
ripidolite	CCa-2	1.405	-0.614	0.965	0.882	0.883	0.852
kaolinite	KGa-1b	12.469	-15.198	7.181	-1.718	4.965	-0.332
illite	IMt-2	4.772	-0.693	3.450	3.588	3.760	4.956
illite/smectite mixed-layer	ISCz-1	11.650	-4.376	9.531	17.084	10.010	6.903
Na-montmorillonite	SWy-2	12.044	-8.134	7.687	0.481	12.207	1.125
Ca-montmorillonite	STx-1b	44.401	-10.915	32.072	7.696	33.032	25.228

### 3.3. Application in Oil-Bearing Shale

The tested amounts ( $q_a$ ) of  $\text{C}_{10}\text{H}_{22}$ ,  $\text{C}_7\text{H}_{14}$  and  $\text{C}_7\text{H}_8$  measured at inflection points for clay minerals have been analyzed above (Table 1); these are assumed to be the adsorbed hydrocarbons. According the weighted average method, the total adsorbed hydrocarbon ( $Q_a$ ) per gram of clay minerals in shale is simply equal to the sum of that ( $q_a$ ) of every clay mineral based on the percentage of clay mineral constituents, expressed as

$$Q_a = \sum_{i=1}^n x_i q_{ai} \quad (3)$$

where  $x_i$  and  $q_{ai}$  are the  $i$ -th clay mineral fraction in shale and its adsorbed hydrocarbon, measured as a percentage and in mg/g, respectively. The  $q_a$  of chlorite is equal to the mean value of  $q_a$  of cookeite and ripidolite. The constraint condition is

$$\sum_{i=1}^n x_i = 1 \quad (4)$$

The clay mineral constituents of shale samples from the Shahejie Formation of the Dongying Sag in the Bohai Bay Basin, China, are mainly illite/smectite mixed-layer (Table 4). Recently, the equilibrium

sorption amount for clay minerals was assigned as 18.0 mg/g on the assessment model of adsorbed and free shale-oil [39,77], which is based on 12 groups of hydrocarbon-solution tests of clay minerals separated from different mudstones/shales in the Shahejie Formation. In this study, the adsorbed amounts ( $Q_a$ ) of  $C_{10}H_{22}$  on clay minerals ranged from 15.40–21.72 mg/g (mean 18.82 mg/g) (Table 4). This range is smaller than that of  $C_7H_{14}$ , with a range of 18.03–28.02 mg/g (mean 23.33 mg/g). Compared to  $C_{10}H_{22}$  and  $C_7H_{14}$ , the adsorbed capacity of  $C_7H_8$  is the smallest, with a range of 10.51–14.60 mg/g (mean 12.78 mg/g).

**Table 4.** Clay mineral constituents and total adsorbed hydrocarbon per gram of clay minerals in shale samples.

Well	Stage	Depth (m)	Clay Mineral Constituents (%)					$Q_a$ (mg/g)		
			K	C	I	S	I/S	$C_{10}H_{22}$	$C_7H_{14}$	$C_7H_8$
B172	Es <sub>3</sub> <sup>x</sup>	3127.30	0	8	20	/	72	17.95	22.16	12.33
F169	Es <sub>4</sub> <sup>s</sup>	3697.00	6	13	26	/	55	15.40	18.03	10.51
F41	Es <sub>3</sub> <sup>x</sup>	2918.66	5	3	14	/	78	19.04	23.60	12.83
H172	Es <sub>3</sub> <sup>x</sup>	3336.80	4	2	19	/	75	18.71	23.03	12.75
H88	Es <sub>3</sub> <sup>x</sup>	3042.60	6	2	19	/	73	18.45	22.54	12.51
L76	Es <sub>4</sub> <sup>s</sup>	3780.42	0	0	3	/	97	21.72	28.02	14.60
LX884	Es <sub>4</sub> <sup>s</sup>	3506.20	0	0	3	/	97	21.72	28.02	14.60
Y556	Es <sub>3</sub> <sup>x</sup>	2448.31	4	3	26	/	67	17.60	21.25	12.13

Es<sub>3</sub><sup>x</sup>: lower-third Member in the Eocene Shahejie Formation; Es<sub>4</sub><sup>s</sup>: upper-fourth Member in the Eocene Shahejie Formation;  $Q_a$ : total adsorbed hydrocarbon per gram of clay minerals; K: kaolinite; C: chlorite; I: illite; S: smectite; I/S: illite/smectite mixed-layer.

#### 4. Conclusions

This study used HVA tests for evaluating the adsorption properties of *n*-decane ( $C_{10}H_{22}$ ), methyl cyclohexane ( $C_7H_{14}$ ) and toluene ( $C_7H_8$ ) on different clay minerals (i.e., cookeite, ripidolite, kaolinite, illite, illite/smectite mixed-layer, Na-montmorillonite and Ca-montmorillonite) at 298.15 K. The results showed the following:

- (1) The tested amounts per unit surface area ( $n_{BET}$ ) measured at inflection points accurately reflects the interaction between clay minerals and hydrocarbons. As a whole, the  $n_{BET}$  for  $C_{10}H_{22}$  ranged from 0.45–1.03 mg/m<sup>2</sup> (mean 0.67 mg/m<sup>2</sup>), and the  $n_{BET}$  for  $C_7H_{14}$  ranged from 0.28–0.90 mg/m<sup>2</sup> (mean 0.42 mg/m<sup>2</sup>).
- (2) The adsorption properties of  $C_{10}H_{22}$ ,  $C_7H_{14}$  and  $C_7H_8$  are associated with the specific surface areas, the pore volumes of mesopores and experimental pressures. In terms of relative specific surface areas and total pore volumes in clay minerals: Ca-montmorillonite > illite/smectite mixed-layer > Na-montmorillonite > illite > cookeite and ripidolite. Kaolinite has a larger pore volume than the illite/smectite mixed-layer, but a smaller specific surface area than illite.
- (3) In the Shahejie Formation, Dongying Sag, Bohai Bay Basin, China, the adsorbed amounts of  $C_7H_{14}$  on clay minerals from shale samples ranges from 18.03–28.02 mg/g (mean 23.33 mg/g), which is larger than that of  $C_{10}H_{22}$ , which ranges from 15.40–21.72 mg/g (mean 18.82 mg/g). The adsorbed capacity of  $C_7H_8$  was the smallest, with a range of 10.51–14.60 mg/g (mean 12.78 mg/g). The values are similar to the adsorption properties of the main clay mineral (i.e., illite/smectite mixed-layer) in the shale samples.

**Acknowledgments:** This study was financially supported by the Key Program of the National Nature Science Foundation (41330313), the National Natural Science Foundation (41602131, 41572122, 41602143), and the Fundamental Research Funds for the Central Universities (17CX06036, 17CX02074, YCX2017002).

**Author Contributions:** J.L. and S.L. conceived and designed the experiments; P.Z. and L.X. performed the experiments; J.Z. and H.X. analyzed the data; X.Z. contributed analysis tools; J.Z. wrote the paper.

**Conflicts of Interest:** The authors declare no conflict of interest.

## References

1. Thomas, M.M.; Clouse, J.A. Selected physical model of secondary oil migration. *AAPG Bull.* **1995**, *79*, 19–29.
2. Li, J.Q.; Liu, D.M.; Yao, Y.B.; Cai, Y.D.; Xu, L.L.; Huang, S.P. Control of CO<sub>2</sub> permeability change in different rank coals during pressure depletion: An experimental study. *Energy Fuels* **2014**, *28*, 987–996. [[CrossRef](#)]
3. Li, J.Q.; Lu, S.F.; Cai, Y.D.; Xue, H.T.; Cai, J.C. Impact of coal ranks on dynamic gas flow: An experimental investigation. *Fuel* **2017**, *194*, 17–26. [[CrossRef](#)]
4. Cai, J.C.; Yu, B.M. A discussion of the effect of tortuosity on the capillary imbibition in porous media. *Transp. Porous Media* **2011**, *89*, 251–263. [[CrossRef](#)]
5. Cai, J.C.; Yu, B.M.; Zou, M.Q.; Luo, L. Fractal characterization of spontaneous co-current imbibition in porous media. *Energy Fuels* **2010**, *24*, 1860–1867. [[CrossRef](#)]
6. Li, J.Q.; Yu, T.; Liang, X.; Zhang, P.F.; Chen, C.; Zhang, J. Insights on the gas permeability change in porous shale. *Adv. Geo-Energ. Res.* **2017**, *1*, 63–67. [[CrossRef](#)]
7. Curtis, J.B. Fractured shale-gas systems. *AAPG Bull.* **2002**, *86*, 1921–1938.
8. Montgomery, S.L.; Jarvie, D.M.; Bowker, K.A.; Pollastro, R.M. Mississippian Barnett shale, Fort Worth basin, north-central Texas: Gas-shale play with multi-trillion cubic foot potential. *AAPG Bull.* **2005**, *89*, 155–175. [[CrossRef](#)]
9. Ross, D.J.K.; Bustin, R.M. Shale gas potential of the Lower Jurassic Gordondale member, northeastern British Columbia. *Canada. Bull. Can. Pet. Geol.* **2007**, *55*, 51–75. [[CrossRef](#)]
10. Chalmers, G.R.L.; Bustin, R.M. Lower Cretaceous gas shales in northeastern British Columbia, Part I: Geological controls on methane sorption capacity. *Bull. Can. Pet. Geol.* **2008**, *56*, 1–21. [[CrossRef](#)]
11. Volzone, C.; Thompson, J.G.; Melnitchenko, A.; Ortiga, J.; Palethorpe, S.R. Selective gas adsorption by amorphous clay-mineral derivatives. *Clays Clay Miner.* **1999**, *47*, 647–657. [[CrossRef](#)]
12. Melnitchenko, A.; Thompson, J.G.; Volzone, C. Selective gas adsorption by metal exchanged amorphous kaolinite derivatives. *Appl. Clay Sci.* **2000**, *17*, 35–53. [[CrossRef](#)]
13. Ji, L.; Zhang, T.; Milliken, K.L.; Qu, J.; Zhang, X. Experimental investigation of main controls to methane adsorption in clay-rich rocks. *Appl. Geochem.* **2012**, *27*, 2533–2545. [[CrossRef](#)]
14. Heller, R.; Zoback, M. Adsorption of methane and carbon dioxide on gas shale and pure mineral samples. *J. Unconv. Oil Gas Resour.* **2014**, *8*, 14–24. [[CrossRef](#)]
15. Cheng, A.L.; Huang, W.L. Selective adsorption of hydrocarbon gases on clays and organic matter. *Org. Geochem.* **2004**, *35*, 413–423. [[CrossRef](#)]
16. Aringhieri, R. Nanoporosity characteristics of some natural clay minerals and soils. *Clays Clay Miner.* **2004**, *52*, 700–704. [[CrossRef](#)]
17. Wang, C.C.; Juang, L.C.; Lee, C.K.; Hsu, T.C.; Lee, J.F. Effects of exchanged surfactant cations on the pore structure and adsorption characteristics of montmorillonite. *J. Colloid Interface Sci.* **2004**, *280*, 27–35. [[CrossRef](#)] [[PubMed](#)]
18. Krooss, B.M.; Van Bergen, F.; Gensterblum, Y.; Siemons, N.; Pagnier, H.J.; David, P. High-pressure methane and carbon dioxide adsorption on dry and moisture equilibrated pennsylvanian coals. *Int. J. Coal Geol.* **2002**, *51*, 69–92. [[CrossRef](#)]
19. Ustinov, E.A.; Do, D.D.; Jaroniec, M. Adsorption of argon and nitrogen in cylindrical pores of MCM-41 materials: Application of density functional theory. *Appl. Surf. Sci.* **2005**, *252*, 1013–1028. [[CrossRef](#)]
20. Ustinov, E.A.; Do, D.D. Comparison of nitrogen adsorption at 77 K on non-porous silica and pore wall of MCM-41 materials by means of density functional theory. *J. Colloid Interface Sci.* **2006**, *297*, 480–488. [[CrossRef](#)] [[PubMed](#)]
21. Zhang, T.; Ellis, G.S.; Ruppel, S.C.; Milliken, K.; Yang, R. Effect of organic-matter type and thermal maturity on methane adsorption in shale-gas systems. *Org. Geochem.* **2012**, *47*, 120–131. [[CrossRef](#)]
22. Wang, S.B.; Song, Z.G.; Cao, T.T.; Song, X. The methane sorption capacity of Paleozoic shales from the Sichuan Basin, China. *Mar. Pet. Geol.* **2013**, *44*, 112–119. [[CrossRef](#)]
23. Gasparik, M.; Bertier, P.; Gensterblum, Y.; Ghanizadeh, A.; Krooss, B.M.; Littke, R. Geological controls on the methane storage capacity in organic-rich shales. *Int. J. Coal Geol.* **2014**, *123*, 34–51. [[CrossRef](#)]
24. Tan, J.; Weniger, P.; Krooss, B.; Merkel, A.; Horsfield, B.; Zhang, J.; Boreham, C.J.; Van Graas, G.; Alastair, B. Shale gas potential of the major marine shale formations in the Upper Yangtze Platform, South China, Part II: Methane sorption capacity. *Fuel* **2014**, *129*, 204–218. [[CrossRef](#)]

25. Hu, H.; Zhang, T.; Wiggins-Camacho, J.D.; Ellis, G.S.; Lewan, M.D.; Zhang, X. Experimental investigation of changes in methane adsorption of bitumen-free Woodford Shale with thermal maturation induced by hydrous pyrolysis. *Mar. Pet. Geol.* **2015**, *59*, 114–128. [[CrossRef](#)]
26. Freundlich, H. Of the adsorption of gases. Section II. Kinetics and energetics of gas adsorption. Introductory paper to section II. *Trans. Faraday Soc.* **1932**, *28*, 195–201. [[CrossRef](#)]
27. Appel, J. Freundlich's adsorption isotherm. *Surf. Sci.* **1973**, *39*, 237–244. [[CrossRef](#)]
28. Langmuir, I. The adsorption of gases on plane surface of glass, mica and platinum. *J. Am. Chem. Soc.* **1918**, *40*, 1361–1403. [[CrossRef](#)]
29. Dubinin, M.M. The potential theory of adsorption of gases and vapors for adsorbents with energetically nonuniform surfaces. *Chem. Rev.* **1960**, *60*, 235–241. [[CrossRef](#)]
30. Dubinin, M.M. Fundamentals of the theory of adsorption in micropores of carbon adsorbents: Characteristics of their adsorption properties and microporous structures. *Pure Appl. Chem.* **1989**, *61*, 1841–1843. [[CrossRef](#)]
31. Chen, S.G.; Yang, R.T. Theoretical basis for the potential theory adsorption isotherms. The Dubinin-Radushkevich and Dubinin-Astakhov equations. *Langmuir* **1994**, *10*, 4244–4249. [[CrossRef](#)]
32. Marlow, B.J.; Sresty, G.C.; Hughes, R.D.; Mahajan, O.P. Colloidal stabilization of clays by asphaltenes in hydrocarbon media. *Colloids Surf.* **1987**, *24*, 283–297. [[CrossRef](#)]
33. Menon, V.B.; Wasan, D.T. Adsorption of maltenes on sodium montmorillonite. *Colloids Surf.* **1987**, *25*, 387–392. [[CrossRef](#)]
34. Kokal, S.; Tang, T.; Schramm, L.; Sayegh, S. Electrokinetic and adsorption properties of asphaltenes. *Colloids Surf. A* **1995**, *94*, 253–265. [[CrossRef](#)]
35. Balabin, R.M.; Syunyaev, R.Z. Petroleum resins adsorption onto quartz sand: Near infrared (NIR) spectroscopy study. *J. Colloid Interface Sci.* **2008**, *318*, 167–174. [[CrossRef](#)] [[PubMed](#)]
36. Daughney, C.J. Sorption of crude oil from a non-aqueous phase onto silica: The influence of aqueous pH and wetting sequence. *Org. Geochem.* **2000**, *31*, 147–158. [[CrossRef](#)]
37. Dudášová, D.; Simon, S.; Hemmingsen, P.V.; Sjöblom, J. Study of asphaltenes adsorption onto different minerals and clays. Part 1. Experimental adsorption with UV depletion detection. *Colloids Surf. A* **2008**, *317*, 1–9. [[CrossRef](#)]
38. Giraldo, J.; Nassar, N.N.; Benjumea, P.; Pereira-almao, P. Modeling and prediction of asphaltene adsorption isotherms using Polanyi's modified theory. *Energy Fuels* **2013**, *27*, 2908–2914. [[CrossRef](#)]
39. Li, Z.; Zou, Y.R.; Xu, X.Y.; Sun, J.N.; Li, M.W.; Peng, P.A. Adsorption of mudstone source rock for shale oil—experiments, model and a case study. *Org. Geochem.* **2016**, *92*, 55–62. [[CrossRef](#)]
40. Marczewski, A.W.; Szymula, M. Adsorption of asphaltenes from toluene on quartz and silica-rich soils. *Colloids Surf. A* **2002**, *58*, 69–79.
41. Minssieux, L.; Nabzar, L.; Chauveteau, G.; Longeron, D. Permeability damage due to asphaltene deposition: Experimental and modeling aspects. *Oil Gas Sci. Technol.* **1998**, *53*, 313–327. [[CrossRef](#)]
42. Mohammadi, M.; Sedigh, M. Modification of Langmuir isotherm for the adsorption of asphaltene or resin onto calcite mineral surface: Comparison of linear and non linear methods. *Prot. Met. Phys. Chem. Surf.* **2013**, *49*, 460–470. [[CrossRef](#)]
43. Montoya, T.; Coral, D.; Franco, C.A.; Nassar, N.N.; Cortés, F.B. A novel solid-liquid equilibrium model for describing the adsorption of associating asphaltene molecules onto solid surfaces based on the “chemical theory”. *Energy Fuels* **2014**, *28*, 4963–4975. [[CrossRef](#)]
44. Pernyeszi, T.; Patzkó, Á.; Berkesi, O.; Dékány, I. Asphaltene adsorption on clays and crude oil reservoir rocks. *Colloids Surf. A* **1998**, *137*, 373–384. [[CrossRef](#)]
45. Ribeiro, R.C.; Correia, J.C.G.; Seidl, P.R. The influence of different minerals on the mechanical resistance of asphalt mixtures. *J. Pet. Sci. Eng.* **2009**, *65*, 171–174. [[CrossRef](#)]
46. Yunan, M.H.; Idris, A.K. Role of asphaltene in changing wettability of reservoir rock. In Proceedings of the Eleventh Symposium of Malaysia Chemical Engineers, Kuala Terengganu, Malaysia, 18–19 June 1995; pp. C12-1–C12-3.
47. Awaja, F.; Bhargava, S. The prediction of clay contents in oil shale using DRIFTS and TGA data facilitated by multivariate calibration. *Fuel* **2006**, *85*, 1396–1402. [[CrossRef](#)]
48. Li, J.Q.; Lu, S.F.; Xie, L.J.; Zhang, J.; Xue, H.T.; Zhang, P.F.; Tian, S.S. Modeling of hydrocarbon adsorption on continental oil shale: A case study on *n*-alkane. *Fuel* **2017**, *206*, 603–613. [[CrossRef](#)]

49. Borden, D.; Giese, R.F. Baseline studies of the clay minerals society source clays: Cation exchange capacity measurements by the ammonia-electrode method. *Clays Clay Miner.* **2001**, *49*, 444–445. [[CrossRef](#)]
50. Chipera, S.J.; David, L.B. Baseline studies of the clay minerals society source clays: Powder x-ray diffraction analyses. *Clays Clay Miner.* **2001**, *49*, 398–409. [[CrossRef](#)]
51. Guggenheim, S.; van Groos, A.F.K. Baseline studies of the clay minerals society source clays: Thermal analysis. *Clays Clay Miner.* **2001**, *49*, 433–443. [[CrossRef](#)]
52. Kogel, J.E.; Lewis, S.A. Baseline studies of the clay minerals society source clays: Chemical analysis by inductively coupled plasma-mass spectroscopy (ICP-MS). *Clays Clay Miner.* **2001**, *49*, 387–392. [[CrossRef](#)]
53. Madejová, J.; Komadel, P. Baseline studies of the clay minerals society source clays: Infrared methods. *Clays Clay Miner.* **2001**, *49*, 410–432. [[CrossRef](#)]
54. Mermut, A.R.; Cano, A.F. Baseline studies of the clay minerals society source clays: Chemical analyses of major elements. *Clays Clay Miner.* **2001**, *49*, 381–386. [[CrossRef](#)]
55. Mermut, A.R.; Lagaly, G. Baseline studies of the clay minerals society source clays: Layer-charge determination and characteristics of those minerals containing 2:1 layers. *Clays Clay Miner.* **2001**, *49*, 393–397. [[CrossRef](#)]
56. Moll, W.F., Jr. Baseline studies of the clay minerals society source clays: Geological origin. *Clays Clay Miner.* **2001**, *49*, 374–380. [[CrossRef](#)]
57. Wu, W.J. Baseline studies of the clay minerals society source clays: Colloid and surface phenomena. *Clays Clay Miner.* **2001**, *49*, 446–452. [[CrossRef](#)]
58. Gailhanou, H.; Rogez, J.; van Miltenburg, J.C.; van Genderen, A.C.G.; Grenèche, J.M.; Gilles, C.; Jalabert, D.; Michau, N.; Gaucher, E.C.; Blanc, P. Thermodynamic properties of chlorite CCa-2. Heat capacities, heat contents and entropies. *Geochim. Cosmochim. Acta* **2009**, *73*, 4738–4749. [[CrossRef](#)]
59. Bustin, R.M.; Clarkson, C.R. Geological controls on coalbed methane reservoir capacity and gas content. *Int. J. Coal Geol.* **1998**, *38*, 3–26. [[CrossRef](#)]
60. Busch, A.; Gensterblum, Y.; Krooss, B.M.; Siemons, N. Investigation of high-pressure selective adsorption/desorption behaviour of CO<sub>2</sub> and CH<sub>4</sub> on coals: An experimental study. *Int. J. Coal Geol.* **2006**, *66*, 53–68. [[CrossRef](#)]
61. Labani, M.M.; Rezaee, R.; Saeedi, A.; Hinai, A.A. Evaluation of pore size spectrum of gas shale reservoirs using low pressure nitrogen adsorption, gas expansion and mercury porosimetry: A case study from the Perth and Canning Basins, Western Australia. *J. Pet. Sci. Eng.* **2013**, *112*, 7–16. [[CrossRef](#)]
62. Barrett, E.P.; Joyner, L.G.; Halenda, P.P. The determination of pore volume and area distributions in porous substances. I. computations from nitrogen isotherms. *J. Am. Chem. Soc.* **1951**, *73*, 373–380. [[CrossRef](#)]
63. Evans, R. The nature of the liquid-vapour interface and other topics in the statistical mechanics of non-uniform classical fluids. *Adv. Phys.* **1979**, *28*, 143–200. [[CrossRef](#)]
64. Sing, K.S.W.; Everett, D.H.; Haul, R.A.W.; Moscou, L.; Pierotti, R.A.; Rouquerol, J.; Siemieniewska, T. Reporting physisorption data for gas/solid systems with special reference to the determination of surface area and porosity. *Pure Appl. Chem.* **1985**, *57*, 603–619. [[CrossRef](#)]
65. Lowell, S.; Shields, J.E. *Powder Surface Area and Porosity*, 2nd ed.; Chapman and Hall: New York, NY, USA, 1984; p. 54. ISBN 978-94-010-8953-1.
66. Gelb, L.D.; Gubbins, K.E.; Radhakrishnan, R.; Sliwinska-Bartkowiak, M. Phase separation in confined systems. *Rep. Prog. Phys.* **1999**, *63*, 727. [[CrossRef](#)]
67. Brunauer, S.; Emmett, P.H.; Teller, E. Adsorption of gases in multimolecular layers. *J. Am. Chem. Soc.* **1938**, *60*, 309–319. [[CrossRef](#)]
68. Groen, J.C.; Peffer, L.A.A.; Pérez-Ramirez, J. Pore size determination in modified micro- and mesoporous materials: Pitfalls and limitations in gas adsorption data analysis. *Microporous Mesoporous Mater.* **2003**, *60*, 1–17. [[CrossRef](#)]
69. Macht, F.; Eusterhues, K.; Pronk, G.J.; Totsche, K.U. Specific surface area of clay minerals: Comparison between atomic force microscopy measurements and bulk-gas (N<sub>2</sub>) and -liquid (EGME) adsorption methods. *Appl. Clay Sci.* **2011**, *53*, 20–26. [[CrossRef](#)]
70. Madsen, F.T. Surface area measurements of clay minerals by glycerol sorption on a thermobalance. *Thermochim. Acta* **1977**, *21*, 89–93. [[CrossRef](#)]
71. Metz, V.; Raanan, H.; Pieper, H.; Bosbach, D.; Ganor, J. Towards the establishment of a reliable proxy for the reactive surface area of smectite. *Geochim. Cosmochim. Acta* **2005**, *69*, 2581–2591. [[CrossRef](#)]

72. Ross, D.J.K.; Bustin, R.M. The importance of shale composition and pore structure upon gas storage potential of shale gas reservoirs. *Mar. Pet. Geol.* **2009**, *26*, 916–927. [[CrossRef](#)]
73. Tournassat, C.; Neaman, A.; Villéras, F.; Bosbach, D.; Charlet, L. Nanomorphology of montmorillonite particles: Estimation of the clay edge sorption site density by low-pressure gas adsorption and AFM observations. *Am. Mineral.* **2003**, *88*, 1989–1995. [[CrossRef](#)]
74. Dogan, A.U.; Dogan, M.; Onal, M.; Sarikaya, Y.; Aburub, A.; Wurster, D.E. Baseline studies of the Clay Minerals Society special clays: Specific surface area by the Brunauer Emmett Teller (BET) method. *Clays Clay Miner.* **2006**, *55*, 534–541. [[CrossRef](#)]
75. Tasi, G.; Pálinkó, I.; Molnár, Á.; Hannus, I. Molecular shape, dimensions, and shape selective catalysis. *J. Mol. Struct. THEOCHEM* **2003**, *666–667*, 69–77. [[CrossRef](#)]
76. McClellan, A.L.; Harnsberger, H.F. Cross-sectional areas of molecules adsorbed on solid surfaces. *J. Colloid Interface Sci.* **1967**, *23*, 577–599. [[CrossRef](#)]
77. Cao, H.; Zou, Y.R.; Lei, Y.; Xi, D.; Wan, X.; Peng, P. Shale oil assessment for the Songliao basin, northeastern China, using oil generation–sorption method. *Energy Fuels* **2017**, *31*, 4826–4842. [[CrossRef](#)]



© 2017 by the authors. Licensee MDPI, Basel, Switzerland. This article is an open access article distributed under the terms and conditions of the Creative Commons Attribution (CC BY) license (<http://creativecommons.org/licenses/by/4.0/>).